Nonlinear stopping effects of slow ions in a no-free-electron system: Titanium nitride

F. Matias

*Centro Atómico Bariloche, Consejo Nacional de Investigaciones Científicas y Técnicas (CONICET),
Avenida E. Bustillo 9500, R8402AGP San Carlos de Bariloche, Río Negro, Argentina*

P. L. Grande

*Instituto de Física, Universidade Federal do Rio Grande do Sul, Avenida Bento Gonçalves, 9500,
CP 15051, CEP 91501-970, Porto Alegre, RS, Brazil*

M. Vos

*Department of Electronic Materials Engineering, Research School of Physics and Engineering,
The Australian National University, Canberra, Australia*

Peter Koval

Donostia International Physics Center, Paseo Manuel de Lardizabal 4, 20018 Donostia-San Sebastián, Spain

Natalia E. Koval

CIC nanoGUNE, Tolosa Hiribidea 76, 20018 San Sebastián, Spain

N. R. Arista

*Centro Atómico Bariloche and Instituto Balseiro, Comisión Nacional de Energía Atómica (CNEA),
Avenida E. Bustillo 9500, R8402AGP San Carlos de Bariloche, Río Negro, Argentina*

A recent experimental study of the energy losses of various ions in titanium nitride, in the low-energy range [M. A. Sortica *et al.*, Sci. Rep. **9**, 176 (2019)], showed a striking departure of the measured values from those predicted by density functional theory. They suggested electron promotion in atomic collisions between dressed atoms as an explanation. In this Rapid Communication, we investigate the process of energy loss of slow ions in TiN using theoretical formulations that are based, on one side, on self-consistent models of nonlinear screening and quantum scattering theory, and on the other, on *ab initio* computations of the electron-density profile of titanium nitride. Two theoretical approaches are considered to determine the average energy transfer: One is based on the local-density approximation for the inhomogeneous electron gas corresponding to the calculated density of TiN, and the other is based on the Penn model for the convolution of the inhomogeneous electron-gas response based on a measured electron-loss function. Both approaches produce very similar results and are in remarkable agreement with the experimental data, indicating that the observed enhancement in the energy-loss values is due to the contribution of a range of electron densities in the TiN compound.

Recent studies on the interaction of ions with solids in the very-low-energy range have produced new and relevant insights in various aspects of the interaction process, including nonlinear screening and band-structure effects [1–6]. In a recent work using light and heavy ions on a TiN target, Sortica *et al.* [7] observed a striking discrepancy in the values of the electronic stopping cross section when compared with the standard predictions of the density functional theory (DFT) [8,9]. The reported effect consists in a strong enhancement of the experimental values with respect to the DFT predictions [7]. They suggested electron promotion in atomic collisions between dressed atoms as an explanation, but so far no calculation or estimation have been done. The purpose of this Rapid Communication is to advance a direct explanation of the effect.

In fact, we provide here two complementary explanations. The first one is based on a self-consistent model for a nonhomogeneous electron gas which is described as a local degenerate Fermi gas [10]. In this approach we use the actual electron-density profile of TiN to obtain quantitative values of the average energy loss of slow ions in this compound. As shown by Calera *et al.* [10], the representation by a nonhomogeneous electron distribution provides a convenient method to account for the contribution of intermediate and inner shells to the average energy loss of slow ions in solids.

For the second explanation, we use recent results by Vos and Grande [11]. They proposed a scheme based on an extension of the dielectric function model to describe the energy loss of ions in solids. In their method, the energy

loss is calculated using the Penn model [12] combined with the transport cross-section (TCS) model, which provides a nonlinear representation of the energy loss. In this method, the target is decomposed as the convolution of electron gases with different local densities.

As we will show here, both methods provide consistent results and explain in quantitative terms the enhancement of the energy-loss values with respect to the DFT predictions, and the attenuation of the oscillatory dependence with Z_1, in very good agreement with the experimental values. If not indicated otherwise, atomic units ($\hbar = m_e = e = 1$) are used throughout this Rapid Communication.

The present approach is based on a previous model proposed by Calera *et al.* [10], which consists in the use of a local-density approximation (LDA) to integrate, for a nonhomogeneous distribution, the results of nonlinear calculations of the energy loss of ions in a homogeneous electron gas. The target is described by its local-density $n(r)$ or equivalently local $r_s(r)$ value, related by $(4\pi/3)r_s^3 = 1/n(r)$. The model makes use of the TCS, which is obtained from a set of self-consistent calculations of scattering phase shifts, by assuming a model potential for the interaction, and subject to the restrictions of the Friedel sum rule [13], namely,

$$Z_1 = \frac{2}{\pi} \sum_{\ell=0}^{\ell_{\max}} (2\ell + 1)\delta_\ell(v_F). \tag{1}$$

In order to apply this model, previous knowledge of the electronic density of the TiN target is necessary. Hence, our first step was to calculate the internuclear distance and the electronic density of the TiN dimer. As described in the work of Sortica *et al.* [7], they used polycrystalline TiN thin films on silicon, which has a NaCl-like (B1) cubic structure. In this structure, the lattice parameter of $a = 8$ a.u. corresponds to the N-Ti-N distance, whose value was calculated from the density $\rho = 5.43$ g/cm^3. In the unit cell, the separation between the Ti and N atoms is given by $d = a/2 = 4$ a.u.

We calculated the electron density of the TiN by means of DFT including explicitly all electrons. The DFT calculation is done using the Python-based simulations of chemistry framework (PYSCF) [14,15] using a Gaussian-type orbital basis set 6-31G [16]. LDA is used to represent the exchange-correlation functional. The calculation is done for the triplet state of the TiN. Moreover, we consider that in the solid (TiN) there are six neighbors that surround each atom, and hence the density is close to the spherically symmetric one. Figure 1 shows the two-dimensional (2D) electron density of the TiN molecule with the internuclear distance $d = 4$ a.u. The Ti atom locates at the origin of the coordinate system ($z = 0$). As can be observed, the density exhibits an approximate spherical symmetry. This fact allows us to get the radial density as a function of the cylindrical coordinate z without deterioration of the electronic properties of TiN, as explained in the following. Figure 2 presents the 1D electron density for the Ti and N atoms as a function of z. As it may be observed in Fig. 2, the value $r_{\text{cut}} = 2$ a.u. (vertical green line) is the interstitial point where the density reaches a minimum, and coincides with half the internuclear distance d. For the sake of reliability, we analyzed the normalization of the electron density to the
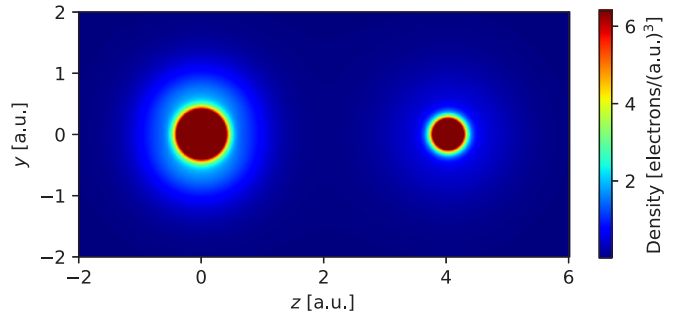

FIG. 1. From the DFT results, we plot the 2D electron density (cut of the density for $x = 0$) for the TiN dimer. The calculates were performed using the Python-based simulations of chemistry framework (PYSCF) code [14,15].

number of electrons in each atom, calculated as

$$N_e = 4\pi \int_0^{r_{\text{cut}}} n(r)r^2 dr. \tag{2}$$

This calculation is performed for the density of the N and Ti atoms shown in Fig. 3, assuming a atomic Wigner-Seitz (WS) sphere around each atom. First, we note that the WS sphere with a cut at $r_{\text{cut}} = 2$ gives a total number of electrons smaller than 29 (the total number of electrons in the TiN dimer). The reason for this is that the WS sphere defined with a radius 2 a.u. has a smaller volume than the cube with sides $2r_{\text{cut}}$ within this cube. Hence, in order to get the correct number of electrons we increase the radius of the WS sphere. We find that $r_{\text{cell}} = 2.38$ gives the correct total number of electrons for the TiN system. It is important to notice that the electronic density is kept constant for values greater than $r = 2$ in both atoms, as can be seen in Fig. 4. This corresponds to a constant electronic density in the interstitial space. By integrating the electron density on each WS cell we obtain 20.50 electrons for the Ti atom and 8.51 electrons for the N atom, with a total number of 29.01 electrons for the TiN system. This means that there is charge transfer from Ti to N, which is reasonable
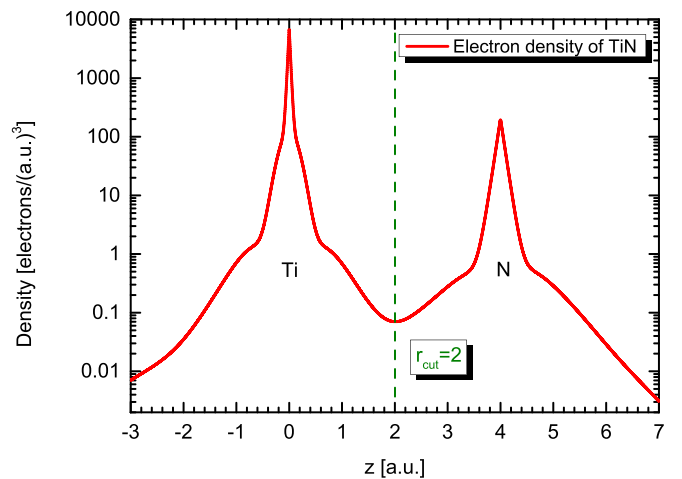

FIG. 2. 1D electron density for the TiN is plotted as a function of the cylindrical coordinate z. The figure was generated assuming $x = y = 0$. $r_{\text{cut}} = 2$ is the cutoff value used to make the spherical mean of the electron density for each of the atoms.
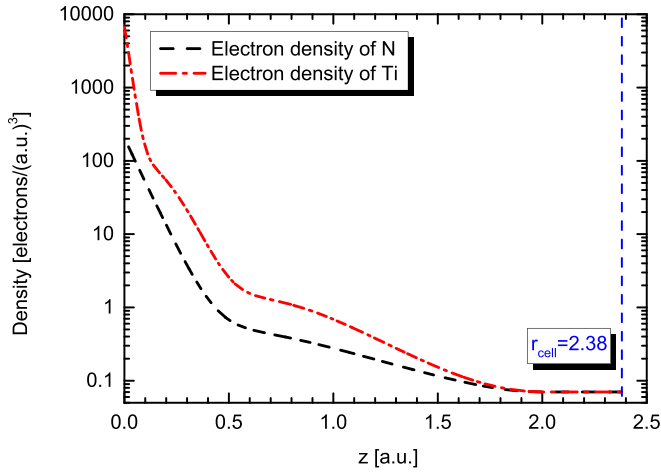
FIG. 3. Plot of the electron density in the WS sphere of each of the atoms. The radial distance $r_{cell} = 2.38$ is the atomic cell radius.

since the N atom is more electronegative. Recently, Magnuson *et al.* [17] found, based on DFT calculations, trends in charge transfer from the 3*d* and 4*s* orbitals of the Ti atom, depending on the electronegativity of the constituent elements of the binary compound. As indicated there, 3*d* orbitals are the main charge reservoir of the Ti-element system, while a smaller amount originates from the 4*s* orbitals. From the distribution of the electronic density in titanium nitride (see Fig. 9, from Ref. [17]), it appears that the mixing of the Ti 3*d* orbitals and the N 2*p* states gives origin to a strong directional covalent bond, giving an indication of the source of the charge received by the N atom. As a general tendency, it was observed that the transition-metal atoms always lose electronic charge, while the electronegative elements as N tend to gain charge. As can be seen in Table 6 from Ref. [17], their calculation yields a charge transfer of 1.41 to the N atom. In comparison, our approach yields a value of 1.5. According to Hug *et al.*, the charge-transfer values depend on the calculation method employed [18]. Therefore, our estimation of the charge-transfer
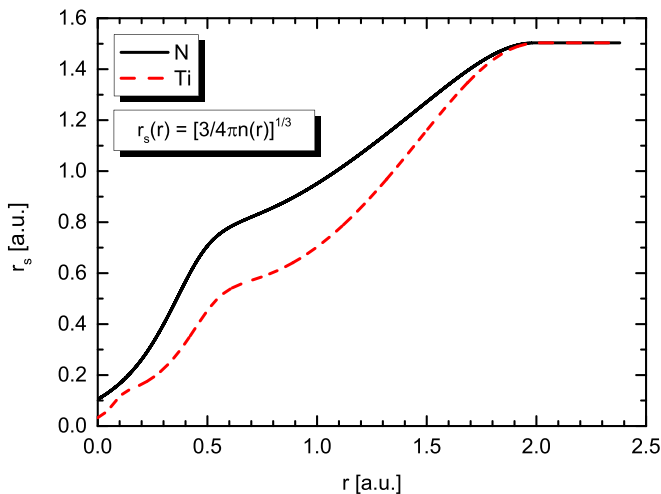

FIG. 4. Plot of the electron-gas parameter r_s as a function of the radial distance r from the nuclei of Ti (black solid line) and N (dashed red line).
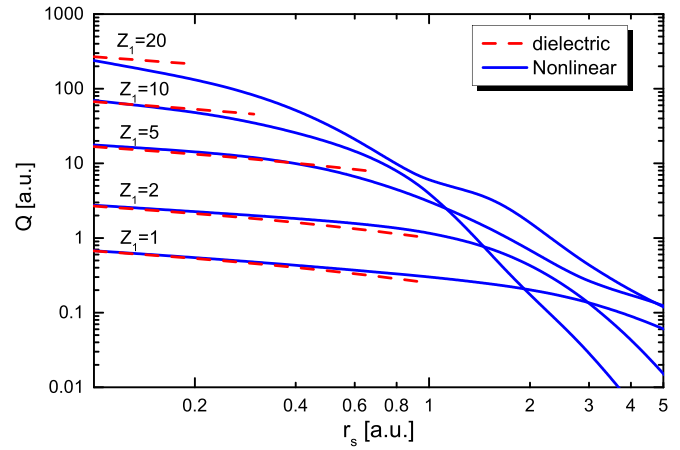

FIG. 5. Values of the low-velocity stopping coefficient S/v as a function of the electron-gas parameter r_s. The blue lines are the results of the TCS-Friedel sum-rule method calculated with Eqs. (3) and (4); the dashed red lines show the results of the dielectric formulation [19,20].

value is in fairly good agreement with the result obtained from the more sophisticated computations of Ref. [17].

Now we first consider the interaction of a projectile with a homogeneous electron gas with density r_s. The calculation of the TCS was made using the method described in Ref. [13]. A model potential, containing only one parameter α, was used. Using this potential, the scattering phase shifts $\delta_\ell(v_F)$ were determined, for a large number of ℓ values, by numerical integrations of the radial Schrödinger equation. The δ_ℓ values so obtained depend on the density parameter r_s (related to the Fermi velocity by $r_s = 1.919/v_F$) and on the potential parameter α. To determine the value of α (for each ion and for each r_s) we require that the δ_ℓ's satisfy the Friedel sum rule.

To comply with this condition a number of iterations are required until a self-consistent solution is obtained. This provides the final values of phase shifts for each combination of Z_1, r_s, and v. This procedure was repeated for r_s values in the range 0.1–1.5, which cover the range of interest for the present study. Then, using the δ_ℓ values so obtained we calculated the TCS, $\sigma_{tr}(Z_1, r_s)$, given by

$$\sigma_{tr}(Z_1, r_s) = \frac{4\pi}{v_F^2} \sum_{\ell=0}^{\ell_{max}} (\ell + 1) \sin^2[\delta_\ell(v_F) - \delta_{\ell+1}(v_F)], \quad (3)$$

and the stopping coefficient

$$Q(Z_1, r_s) = S(Z_1, r_s)/v = n(r) v_F \sigma_{tr}(Z_1, r_s), \quad (4)$$

for all those cases.

As an example, we show in Fig. 5 the results for the stopping coefficient, for various Z_1, as a function of r_s. For small r_s values, the results of the full quantum mechanical formulation (TCS results) approach those of the linear (dielectric) formulation, but show a strong nonlinear behavior with increasing r_s. The final step in this approach is to integrate the stopping coefficient over the WS cells corresponding to

the Ti and N atoms, using the expression

$$Q_{\mathrm{Ti,N}}(Z_1) = N_a \int_0^{r_{\mathrm{cell}}} d^3 r Q(Z_1, r_s(r)), \qquad (5)$$

where r_{cell} is the atomic cell radius, and N_a the number of Ti,N atoms per unit volume. The values of $r_s(r)$ are found in Fig. 4. This form of spherical average was first proposed by Bonderup [21] (in the context of a statistical atomic model) and was further used by others (see, for instance, Ref. [22] for further references), considering linear models for the local energy loss. In the present context, our approach is based on previous work by Calera *et al.* [10], who proposed a similar cell average using nonlinear TCS calculations based on the Friedel sum rule. Finally, in order to compare with the experiments, we calculate the so-called "stopping effective charge" using Brandt's definition [23–25], which in this case may be written as

$$Z_1^* = \sqrt{\frac{Q_s(Z_1)}{Q_s(Z_1 = 1)}}, \qquad (6)$$

where $Q_s(Z_1) = Q_{\mathrm{Ti}}(Z_1) + Q_{\mathrm{N}}(Z_1)$. This definition of Z_1^* was suggested for high-energy ions because of the Z_1^2 dependence of the TCS. Here, for low-energy ions, Z_1^* cannot be used as an ion charge in any stopping formula.

Another nonlinear approach to describe the stopping power of heavy ions in matter has been proposed recently [11]. In this model the effects of nonfree-electron distributions are incorporated in the TCS model by taking into account the superposition of electron-gas responses with different densities as described for the Penn method [12]. For this sake each electron-gas density is weighted according to the energy-loss function (ELF) of the material in the optical limit as

$$g(\omega_p) = \frac{2}{\pi \omega_p} \mathrm{ELF}(\omega_p), \qquad (7)$$

where each electron-gas contribution is described by the plasmon frequency ω_p obtained from r_s as $\omega_p = \sqrt{3} r_s^{-3/2}$. The stopping power is then given by

$$S_{\mathrm{TCS\text{-}Penn}} = \int_0^\infty d\omega_p g(\omega_p) S_{\mathrm{TCS}}(Z_1, r_s), \qquad (8)$$

with the stopping $S_{\mathrm{TCS}}(Z_1, r_s)$ given in terms of the transport cross section according to Eq. (3).

In order to provide a best comparison with the experimental data we measured an electron energy-loss spectrum of TiN for the same samples used in the original experiments [5]. For 5 keV incoming electron energy the energy-loss spectrum was dominated by the top TiN layer (thickness 17.5 nm), but the energy was still high enough so that the contribution of surface plasmons is small and could be neglected. Using the PM3 program [26] the energy-loss spectrum was calculated. This Monte Carlo program simulates the electron trajectories, including the elastic deflection of nuclei and inelastic excitations of the target electrons based on the dielectric function. The dielectric function, expressed as a sum of Mermin oscillators, was varied so a reasonable description of the experiment is obtained (see Fig. 6) and the Bethe sum corresponds to 17 electrons per unit cell (the appropriate number of valence electrons, without the N 1*s* and Ti 1*s*, 2*s*, and 2*p* electrons which contribute to the ELF at larger energy losses). The

TABLE I. The amplitude (A_i) width (Γ_i), and energy (ω_i) of the Mermin oscillators used here to describe the dielectric function of TiN.

i	A_i	Γ_i	ω_i
1	0.13	1	2.3
2	0.023	5	7
3	0.05	4	12.1
4	0.12	5	16.3
5	0.009	2	19.5
6	0.38	8	25.3
7	0.005	3	38.5
8	0.071	10	44
9	0.16	10	51
10	0.033	140	100

corresponding ELF (energy-loss function at $q = 0$) is given in Table I and shown in Fig. 6 as well, where it is compared with previous estimates of the same quantity.

Following the prescriptions of the TCS-LDA model, Eqs. (5) and (6) were calculated for ions in the range of atomic numbers $Z_1 = 1$–20 for the electron densities corresponding to the Ti and N atoms, as described before. The results are shown in Figs. 7 and 8.

In Fig. 7 we show the results of the stopping cross section for the six elements measured in Ref. [7]. In the cases of H and He our calculations are in excellent agreement with the experimental values. The results for Al are also in good
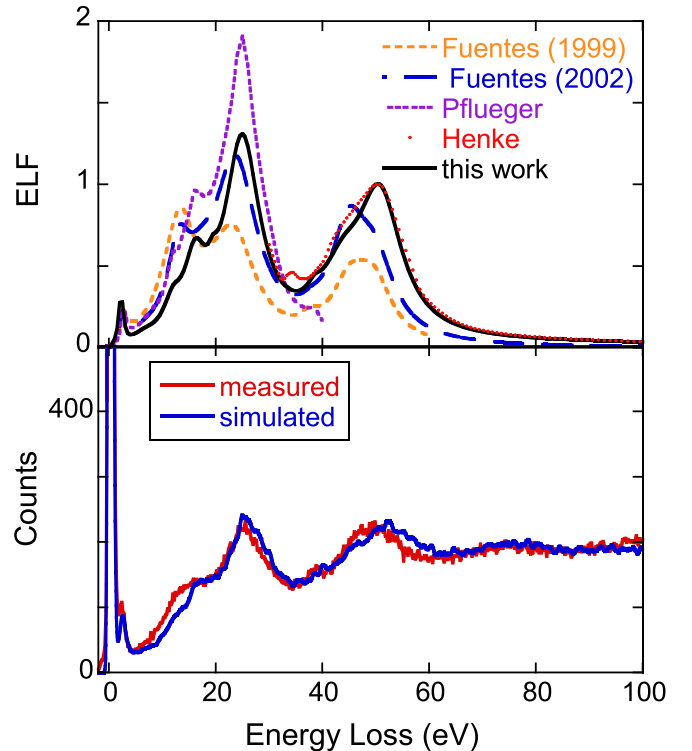

FIG. 6. Top: The assumed ELF compared to previous estimates of Fuentes (1999) [27], Fuentes (2002) [28], Pflüger [29], and Henke [30]. Bottom: The simulated electron energy-loss spectra at 5 keV compared to the experimentally obtained one.
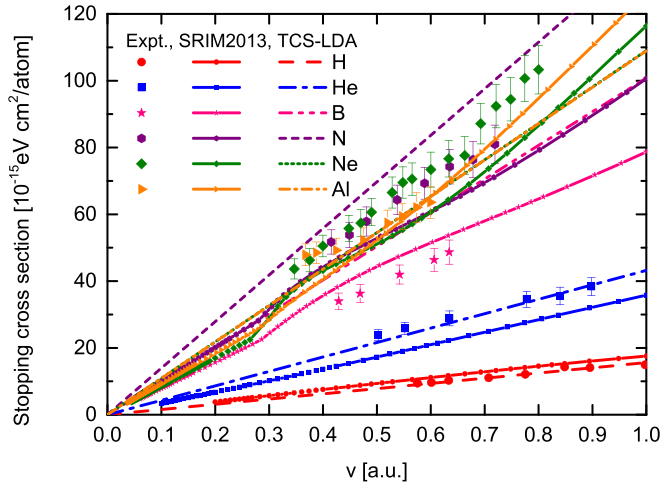
FIG. 7. The theoretical results of the TCS-LDA approach for the stopping cross section of H, He, B, N, Ne, and Al ions in TiN (lines). For comparison, the experimental data from Sortica *et al.* [7] (solid symbols), and the semiempirical results of SRIM are plotted as well.

agreement, while for Ne our values are lower (by about 10% at the lowest energies), but are still better than the stopping and range of ions in matter (SRIM) values through the measured energy range. (We must notice that the theoretical results for Al and Ne are almost coincident so that the two curves merge in this graph.) Similar deviations are observed for N; in this case our results are about 10%–15% larger at the lowest energies while the SRIM values are lower by about the same percentage. The largest deviations are observed for B ions where our calculations are 26% larger at lowest energies; this is the only case where the semiempirical results of SRIM compare better with the experiment.

Figure 8 shows the results of the effective charge obtained from Eq. (6) as a function of the ion atomic number Z_1. We
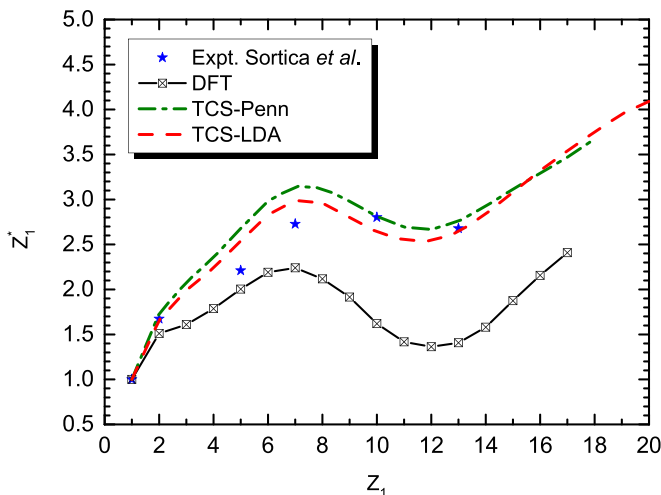

FIG. 8. Calculated values of the effective charge Z_1^* using the TCS-LDA and TCS-Penn methods (red and green lines), together with the experimental results from Ref. [7]. The lower black curve shows the results of the standard DFT calculations [9] for a constant r_s value equal to 1.61.

also show in this figure the results obtained from the TCS-Penn model, as well as the experimental results from Ref. [7] and previous theoretical predictions from DFT [9] assuming an r_s value of 1.61, appropriate for the valence electrons of TiN.

We find here a remarkable agreement between all the results (except for the DFT value with fixed r_s). On one side, we find very close agreement between the TCS-LDA (dashed red curve) and TCS-Penn (dashed-dotted green curve) models; on the other side, both models show excellent agreement with the experimental data (blue symbols) of Sortica *et al.* [7], reproducing both the shape and the absolute values of the experiment. We notice that the nonhomogeneity of the electron gas is an essential factor for the more accurate description of the average energy loss in this material. For this reason, the attempt to represent the electronic structure of the titanium nitride by an effective r_s parameter shows strong disagreement with the experiment.

Stimulated by recent experimental results of the energy loss of various ions in TiN, we have made a detailed theoretical investigation of the energy-loss process. Our study is based on nonlinear models for the energy-transfer and *ab initio* calculations of the electronic density of TiN. We find a remarkable agreement between the experimental and our theoretical results. On one side, we find a very close agreement between both model calculations (TCS-LDA and TCS-Penn models), which have, as the only common ingredient, numerical calculations based on nonlinear screening and quantum scattering theory. The basic theoretical model is a self-consistent approach where the scattering phase shifts are obtained from numerical solutions of the radial Schrödinger equation using the exact Friedel sum rule as the only fitting criterion. The additional theoretical assumption is the LDA which permits one to integrate the average energy loss using the real electron density of the TiN sample obtained from *ab initio* calculations. The most remarkable feature of both theoretical approaches is the very close agreement with the experimental data.

In summary, the present calculations provide a quantitative theoretical explanation of the enhancement of the experimental energy-loss values with increasing Z_1 and the attenuation of the oscillatory dependence on Z_1. Our calculations show that this behavior is produced by the effects of intermediate densities in the electronic structure of TiN, corresponding mainly to r_s values in the range 0.5–1.5. This range (actually 0.7–1.0) corresponds to the second peak in the ELF function displayed in the top panel of Fig. 6.

Finally, this explains the previously observed discrepancy with the more restricted DFT calculations that assumed a constant r_s value appropriate only for the valence electrons of TiN. A comparison with *ab initio* calculations such as time-dependent DFT (TDDFT) [6] will be useful to demonstrate the strength of present theoretical formalisms.

[1] J. M. Pruneda, D. Sánchez-Portal, A. Arnau, J. I. Juaristi, and E. Artacho, Phys. Rev. Lett. **99**, 235501 (2007).

[2] D. Goebl, W. Roessler, D. Roth, and P. Bauer, Phys. Rev. A **90**, 042706 (2014).

[3] D. Roth, B. Bruckner, M. V. Moro, S. Gruber, D. Goebl, J. I. Juaristi, M. Alducin, R. Steinberger, J. Duchoslav, D. Primetzhofer, and P. Bauer, Phys. Rev. Lett. **118**, 103401 (2017).

[4] D. Roth, B. Bruckner, G. Undeutsch, V. Paneta, A. I. Mardare, C. L. McGahan, M. Dosmailov, J. I. Juaristi, M. Alducin, J. D. Pedarnig *et al.*, Phys. Rev. Lett. **119**, 163401 (2017).

[5] M. A. Sortica, V. Paneta, B. Bruckner, S. Lohmann, M. Hans, T. Nyberg, P. Bauer, and D. Primetzhofer, Phys. Rev. A **96**, 032703 (2017).

[6] R. Ullah, E. Artacho, and A. A. Correa, Phys. Rev. Lett. **121**, 116401 (2018).

[7] M. A. Sortica, V. Paneta, B. Bruckner, S. Lohmann, T. Nyberg, P. Bauer, and D. Primetzhofer, Sci. Rep. **9**, 176 (2019).

[8] M. J. Puska and R. M. Nieminen, Phys. Rev. B **27**, 6121 (1983).

[9] P. M. Echenique, R. M. Nieminen, J. C. Ashley, and R. H. Ritchie, Phys. Rev. A **33**, 897 (1986).

[10] J. Calera-Rubio, A. Gras-Martí, and N. R. Arista, Nucl. Instrum. Methods Phys. Res., Sect. B **93**, 137 (1994).

[11] M. Vos and P. Grande, J. Phys. Chem. Solids **133**, 187 (2019).

[12] D. R. Penn, Phys. Rev. B **35**, 482 (1987).

[13] A. F. Lifschitz and N. R. Arista, Phys. Rev. A **57**, 200 (1998).

[14] Q. Sun, T. C. Berkelbach, N. S. Blunt, G. H. Booth, S. Guo, Z. Li, J. Liu, J. D. McClain, E. R. Sayfutyarova, S. Sharma *et al.*, WIREs Comput. Mol. Sci. **8**, e1340 (2018).

[15] P. Koval, M. Barbry, and D. Sánchez-Portal, Comput. Phys. Commun. **236**, 188 (2019).

[16] V. A. Rassolov, J. A. Pople, M. A. Ratner, and T. L. Windus, J. Chem. Phys. **109**, 1223 (1998).

[17] M. Magnuson and M. Mattesini, Thin Solid Films **621**, 108 (2017).

[18] G. Hug, M. Jaouen, and M. W. Barsoum, Phys. Rev. B **71**, 024105 (2005).

[19] J. Lindhard, Mat. Fys. Medd. Dan. Vid. Selsk. **28**, 1 (1954).

[20] J. Lindhard and A. Winther, *Stopping Power of Electron Gas and Equipartition Rule*, K. Dan. Vidensk. Selsk., Mat.-Fys. Medd. Vol. 34 (Ejnar Munksgaard, Copenhagen, 1964).

[21] E. Bonderup, Mat. Fys. Medd. Dan. Vid. Selsk. **35**, 1 (1967).

[22] C. J. Tung, J. C. Ashley, and R. H. Ritchie, Surf. Sci. **81**, 427 (1979).

[23] W. Brandt, *Atomic Collisions in Solids* (Plenum, New York, 1973), Vol. 1, p. 261.

[24] B. S. Yarlagadda, J. E. Robinson, and W. Brandt, Phys. Rev. B **17**, 3473 (1978).

[25] J. Ziegler, J. Biersack, and U. Littmark, *The Stopping and Range of Ions in Solids* (Pergamon, New York, 1985).

[26] G. Marmitt, Metal oxides of resistive memories investigated by electron and ion backscattering, Ph.D. thesis, Universidade Federal do Rio Grande do Sul, 2017, https://www.lume.ufrgs.br/bitstream/handle/10183/170451/001053460.pdf?sequence=1.

[27] G. G. Fuentes, I. G. Mancheño, F. Balbás, C. Quirós, J. F. Trigo, F. Yubero, E. Elizalde, and J. M. Sanz, Phys. Status Solidi A **175**, 429 (1999).

[28] G. G. Fuentes, E. Elizalde, F. Yubero, and J. M. Sanz, Surf. Interface Anal. **33**, 230 (2002).

[29] J. Pflüger, J. Fink, W. Weber, K. P. Bohnen, and G. Crecelius, Phys. Rev. B **30**, 1155 (1984).

[30] B. Henke, E. Gullikson, and J. Davis, At. Data Nucl. Data Tables **54**, 181 (1993).